# Seeded growth of $\beta$-amyloid fibrils from Alzheimer's brain-derived fibrils produces a distinct fibril structure

Anant K. Paravastu[a,1], Isam Qahwash[b], Richard D. Leapman[c], Stephen C. Meredith[b], and Robert Tycko[a,2]

[a]Laboratory of Chemical Physics, National Institute of Diabetes and Digestive and Kidney Diseases, National Institutes of Health, Bethesda, MD 20892-0520; [b]Department of Biochemistry and Molecular Biology and Department of Pathology, The University of Chicago, Chicago, IL 60637; and [c]Laboratory of Bioengineering and Physical Science, National Institute of Biomedical Imaging and Bioengineering, National Institutes of Health, Bethesda, MD 20892-5766

Edited by Ann E. McDermott, Columbia University, New York, NY, and approved March 11, 2009 (received for review November 25, 2008)

**Studies by solid-state nuclear magnetic resonance (NMR) of amyloid fibrils prepared *in vitro* from synthetic 40-residue $\beta$-amyloid ($A\beta_{1-40}$) peptides have shown that the molecular structure of $A\beta_{1-40}$ fibrils is not uniquely determined by amino acid sequence. Instead, the fibril structure depends on the precise details of growth conditions. The molecular structures of $\beta$-amyloid fibrils that develop in Alzheimer's disease (AD) are therefore uncertain. We demonstrate through thioflavin T fluorescence and electron microscopy that fibrils extracted from brain tissue of deceased AD patients can be used to seed the growth of synthetic $A\beta_{1-40}$ fibrils, allowing preparation of fibrils with isotopic labeling and in sufficient quantities for solid-state NMR and other measurements. Because amyloid structures propagate themselves in seeded growth, as shown in previous studies, the molecular structures of brain-seeded synthetic $A\beta_{1-40}$ fibrils most likely reflect structures that are present in AD brain. Solid-state $^{13}C$ NMR spectra of fibril samples seeded with brain material from two AD patients were found to be nearly identical, indicating the same molecular structures. Spectra of an unseeded control sample indicate greater structural heterogeneity. $^{13}C$ chemical shifts and other NMR data indicate that the predominant molecular structure in brain-seeded fibrils differs from the structures of purely synthetic $A\beta_{1-40}$ fibrils that have been characterized in detail previously. These results demonstrate a new approach to detailed structural characterization of amyloid fibrils that develop in human tissue, and to investigations of possible correlations between fibril structure and the degree of cognitive impairment and neurodegeneration in AD.**

Alzheimer's disease | electron microscopy | solid-state nuclear magnetic resonance

The molecular structure of amyloid fibrils formed *de novo* by the $\beta$-amyloid peptide associated with AD depends on fibril growth conditions (1–3). The ability of preformed fibrils to propagate their structures through seeded growth *in vitro* has enabled detailed structural characterization of two distinct $A\beta_{1-40}$ fibril structures, based largely on solid-state NMR measurements on a series of $^{15}N$- and $^{13}C$-labeled samples (4, 5). Self-propagating, molecular-level structural polymorphism of amyloid fibrils underlies the phenomenon of strains in yeast prions and possibly mammalian prions (6–8). Amyloid polymorphism may also play a role in human amyloid diseases, for example by controlling the toxicity of amyloid deposits (1, 9). Detailed structural characterization of amyloid fibrils that develop *in vivo* may help to elucidate the role of fibrils in human disease, which is presently a subject of controversy (10, 11). However, direct structural measurements are prevented by the small quantities and lack of isotopic labels in fibrils formed *in vivo*.

Here we report seeded growth of $A\beta_{1-40}$ fibrils from fibrils that were extracted from frontal lobe brain tissue, obtained at autopsy, from two AD patients., Fibril extraction follows a previously reported protocol (12), with modifications described below. Thioflavin T (ThT) fluorescence and transmission electron microscopy (TEM) measurements show a clear acceleration of the conversion of synthetic $A\beta_{1-40}$ to fibrillar form upon addition of AD brain-derived material, i.e., a clear seeding effect. Because previous *in vitro* experiments have shown that seeded fibril growth generally preserves molecular structure (1), the structures of brain-seeded fibrils most likely correspond to structures present in AD brain. Moreover, seeded growth from brain-derived material permits us to prepare isotopically labeled fibrils in the milligram quantities required for solid-state NMR.

Solid-state NMR measurements on fibrils seeded with material from two separate AD patients (brains 1 and 2; see Materials and Methods) yield the same results, as described below: (*i*) brain-seeded $A\beta_{1-40}$ fibrils have the same two coexisting molecular structures, with one structure being predominant; (*ii*) the predominant structure in brain-seeded fibrils is different from the two $A\beta_{1-40}$ fibril structures that we have characterized in detail in previous work on purely synthetic samples (4, 5). Parallel control experiments show that unseeded fibril growth produces greater structural heterogeneity, supporting the hypothesis that specific fibril structures are present in AD brain, leading to specific structures in the brain-seeded samples. These results indicate the feasibility of using seeded growth in combination with solid-state NMR and other physical techniques to determine the molecular structures of fibrils that develop *in vivo* in AD and other amyloid diseases.

## Results

**Seeding of Synthetic $A\beta_{1-40}$ Fibril Growth by Brain Amyloid.** TEM images of amyloid material extracted from AD brain show both fibrils and residual nonfibrillar material (Figs. 1*A*–1*C*). Western blotting with monoclonal antibody 6E10, which recognizes residues 3–8 of the $\beta$-amyloid peptide, confirmed the identity of these fibrils. The fibrils have diameters and morphologies similar to those of synthetic $\beta$-amyloid fibrils (1, 2), but the precise morphologies of fibrils in brain amyloid are difficult to assess because of self-association of fibrils and adherence of masses of nonfibrillar particles. $\beta$-Amyloid from brain tissue presumably includes the chain length variants and chemical modifications identified previously (13).

The ability of AD brain amyloid to accelerate fibril formation in synthetic $A\beta_{1-40}$ solutions (i.e., to act as a seed) was demonstrated by both TEM and ThT fluorescence measurements. For TEM measurements, brain amyloid was sonicated and added to solutions of synthetic $A\beta_{1-40}$, in an approximate 1:20 molar ratio of brain-derived $\beta$-amyloid to synthetic $A\beta_{1-40}$. TEM images obtained 4

Author contributions: A.K.P., I.Q., S.C.M., and R.T. designed research; A.K.P., I.Q., and R.D.L. performed research; A.K.P., I.Q., R.D.L., S.C.M., and R.T. analyzed data; and A.K.P., S.C.M., and R.T. wrote the paper.

The authors declare no conflict of interest.

This article is a PNAS Direct Submission.

[1]Current address: Department of Chemical and Biomedical Engineering, Florida A&M University-Florida State University College of Engineering, Tallahassee, FL 32310-6046.

[2]To whom correspondence should be addressed. E-mail: robertty@mail.nih.gov.

This article contains supporting information online at www.pnas.org/cgi/content/full/0812033106/DCSupplemental.

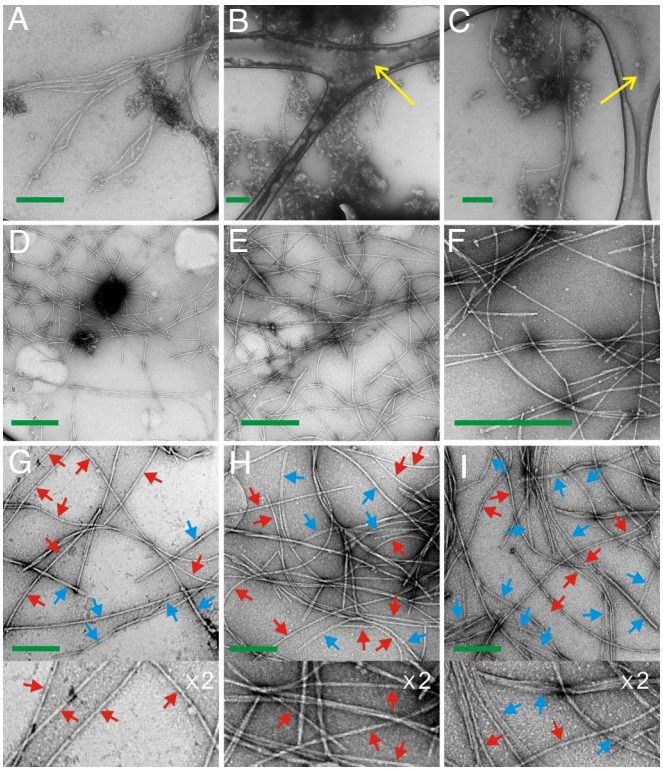


**Fig. 1.** Negatively stained TEM images of β-amyloid fibrils. (*A-C*) Fibrils extracted from AD brain tissue. Yellow arrows indicate carbon lace of the sample grid. (*D-F*) $A\beta_{1-40}$ fibrils observed 4 hours after seeding of a monomeric $A\beta_{1-40}$ solution with AD brain amyloid. (*G-I*) $A\beta_{1-40}$ fibrils in the brain 1/generation 3, brain 2/generation 3, and control/generation 3 samples, respectively. Red arrows indicate the predominant fibril morphology in brain-seeded samples. Blue arrows indicate other morphologies. Green scale bars, 400 nm.

hours after initial seeding reveal the presence of long (several micrometers) fibrils (Figs. 1*D*–1*F*). In contrast, no fibrils were observed in a parallel unseeded control solution of synthetic $A\beta_{1-40}$ after 24 hours, using identical TEM conditions. As expected, fibrils were detected by TEM in the control solution after longer incubation periods (>48 hours).

Results of ThT fluorescence experiments are shown in Fig. 2. The

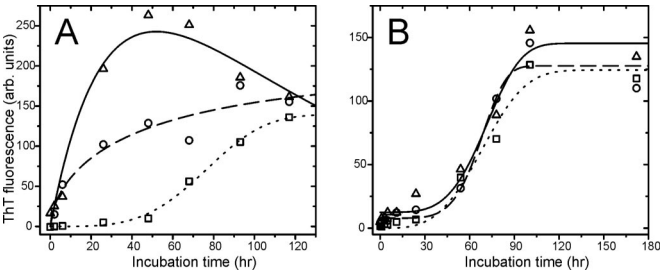


**Fig. 2.** Amyloid fibril formation kinetics monitored by ThT fluorescence. (*A*) Unseeded $A\beta_{1-40}$ solution (open square and dotted line) and solutions seeded with sonicated synthetic $A\beta_{1-40}$ fibrils (open circles and dashed line) or sonicated amyloid from brain 2 (open triangles and solid line). Brain amyloid data are scaled down by a factor of 2. (*B*) Unseeded $A\beta_{1-40}$ solution (open squares and dotted line) and solutions seeded with brain material from a non-demented, 25-year-old man (open circles and dashed line) or a non-demented, 56-year-old woman (open triangles and solid line). Lines are empirical fits with a stretched exponential function (dotted line in A, all lines in *B*), a monoexponential function (dashed line in *A*), and the difference between two monoexponential functions (solid line in A).

kinetics of fibril growth in unseeded solutions of monomeric $A\beta_{1-40}$, as monitored by ThT fluorescence, can be fit empirically by a stretched exponential equation of the form $F(t) = F_0 + (F_\infty - F_0)[1 - e^{-(t/\tau)^s}]$ with $s > 1$, corresponding to an initial lag period of low fluorescence, a maximal rate of increase at $t = (s - 1/s)^{1/s}\tau$, and a plateau at long incubation times (14). For unseeded experiments in Fig. 2, $s \approx 3.5$ and $\tau \approx 80$ hours. Figure 2*A* shows that addition of either synthetic $A\beta_{1-40}$ fibril fragments or sonicated brain amyloid eliminated the lag period. Seeding with synthetic fibrils resulted in monoexponential kinetics ($s = 1$, $\tau \approx 24$ h). Seeding with brain amyloid produced significantly greater ThT fluorescence and non-monotonic kinetics, possibly because of fibril–fibril association and blockage of ThT binding sites at long times. Similar non-monotonic kinetics have been reported for a modified $A\beta_{1-40}$, i.e., K28-octanoyl-$A\beta_{1-40}$ (15). Figure 2*B* shows that material extracted from brain tissue of two patients without AD, which contained nonfibrillar particles but no amyloid fibrils detectable by TEM, did not seed or accelerate $A\beta_{1-40}$ fibril growth.

**Fibril Amplification by Seeded Growth.** The first round of brain-seeded growth (or unseeded growth in the case of the control sample) produced "generation 1" fibrils. Two subsequent rounds of seeded growth (using generations 1 and 2 as seeds to produce generations 2 and 3, respectively) resulted in amplification (factor of 10–20 per generation) to quantities necessary for solid-state NMR. Generation 3 fibrils were produced with isotopically labeled $A\beta_{1-40}$ to allow solid-state NMR measurements. In TEM images of brain 1/generation 3 and brain 2/generation 3 samples, the most prevalent fibrils (red arrows in Figs. 1*G* and 1*H*) are single filaments with apparent widths of 6.5 ± 1.0 nm, without an obvious width modulation. Other morphologies (blue arrows) include fibrils with periodic width modulations (50–120 nm spacing between apparent width maxima) and fibrils with 10–15 nm widths that are apparently formed by lateral association of finer filaments. We call the latter morphology a "striated ribbon" (4, 5). TEM images of the control/generation 3 sample (Fig. 1*I*) reveal a greater mixture of morphologies, with an apparently larger proportion of striated ribbons.

Energy-filtered TEM (EFTEM) was used as described by Feja et al. (16) to measure the mass-per-length (MPL) distribution of brain 2/generation 3 fibrils [supporting information (SI) Fig. S1]. MPL values were in the 15–33 kDa/nm range, similar to MPL data for purely synthetic $A\beta_{1-40}$ fibrils (1, 4, 17). Given the 0.48-nm intermolecular spacing in the β-sheets of amyloid fibrils and the 4.3 kDa molecular weight, a single layer of $A\beta_{1-40}$ molecules would have MPL ≈ 9 kDa/nm. Brain-seeded $A\beta_{1-40}$ fibril samples therefore contain fibrils with both two and three molecular layers. MPL data for synthetic $A\beta_{1-40}$ fibrils (1, 4) have shown that striated ribbon fibrils contain multiples of two molecular layers (MPL ≈ 18 kDa/nm, 36 kDa/nm, etc.), whereas fibrils with a pronounced width modulation in negatively stained TEM images (called "twisted fibrils") contain three molecular layers (MPL ≈ 27 kDa/nm). Data in Fig. S1 suggest that the most prevalent fibril structure in brain-seeded samples may contain three molecular layers, although the apparent abundances of different fibril structures may be affected by differences in self-association or adsorption to the TEM grid.

**Characterization of Molecular Structure by Solid-State NMR.** Two-dimensional (2D) $^{13}C$ NMR spectra of generation 3 fibrils, with uniform $^{15}N$,$^{13}C$-labeling of F19, V24, G25, A30, I31, L34, and M35, are shown in Fig. 3. These spectra were obtained with magic-angle spinning (MAS) and with finite-pulse radiofrequency–driven recoupling (fpRFDR) in the mixing period (1, 4, 18), producing strong one-bond crosspeaks that allow site-specific assignments of $^{13}C$ NMR chemical shifts. Both brain-seeded samples show two sets of chemical shifts for many $^{13}C$-labeled sites, indicating coexistence of two unequally populated fibril structures. Integration of majority and minority crosspeak components indicates that the minority

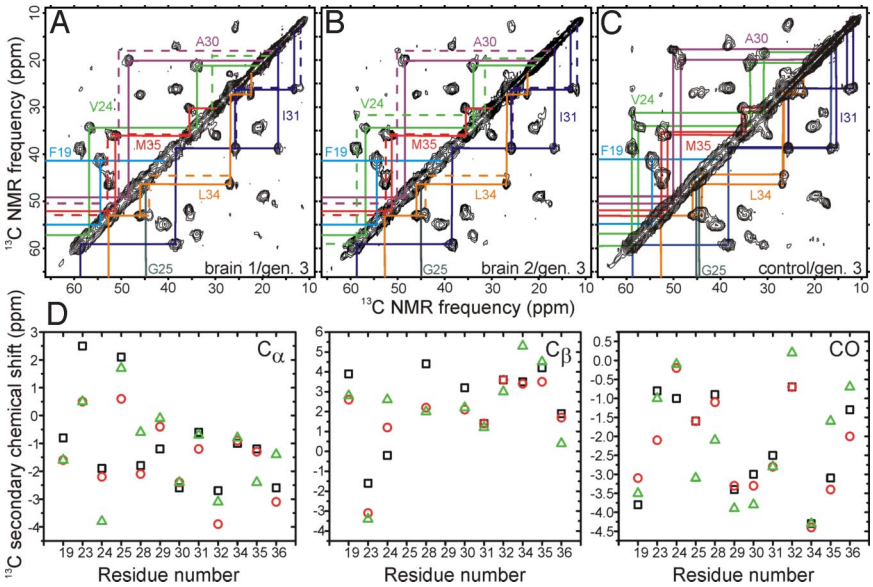


**Fig. 3.** 2D solid-state $^{13}$C NMR spectra of A$\beta_{1-40}$ fibrils. (*A-C*) Aliphatic regions of spectra for brain 1/generation 3, brain 2/generation 3, and control/generation 3. Fibrils were uniformly $^{15}$N,$^{13}$C-labeled at F19, V24, G25, A30, I31, L34, and M35. Chemical shift assignment paths are shown, with solid and dashed lines in (*A*) and (*B*) indicating majority and minority signals, respectively. The distinction between majority and minority signals is unclear in (*C*). (*D*) Comparison of secondary shifts (i.e., deviations from random coil values) for brain-seeded fibril majority signals (brain 1/generation 3, green triangles) with previously reported secondary shifts for purely synthetic fibrils with twisted (red circles) and striated ribbon (black squares) morphologies.

structure accounts for 20 ± 10% of the fibrils in the brain 1/generation 3 sample and 30 ± 5% in the brain 2/generation 3 sample. Crosspeak positions and lineshapes for majority and minority structures are the same in both brain-seeded samples, to within experimental error. In contrast, the 2D $^{13}$C NMR spectrum of the control/generation 3 sample contains significantly broader lines and nearly equal intensities of two or more crosspeak components, indicating greater structural inhomogeneity and the absence of a clear majority structure. Direct overlays of the 2D spectra and comparisons of one-dimensional (1D) slices from these spectra (Fig. S2) support the close similarity of the $^{13}$C NMR chemical shifts and lineshapes for two brain-seeded samples, and the dissimilarity of the control/generation 3 NMR data.

$^{13}$C NMR chemical shifts are listed in Table S1. The root-mean-squared deviation between chemical shifts for majority (minority) signals from the two brain-seeded samples is 0.04 ppm (0.07 ppm), less than the $^{13}$C NMR linewidths by a factor of 25. The root-mean-squared deviation between brain 1/generation 3 and control/generation 3 chemical shifts is significantly greater, being 0.28 ppm for majority and 0.44 ppm for minority signals (using signals in the control/generation 3 spectrum that are closest to corresponding signals in the brain 1/generation 3 spectrum). Because $^{13}$C NMR chemical shifts are sensitive to peptide conformation and structural environment, these results show that the two brain-seeded samples have the same majority and minority structures. The most prevalent structures in the control/generation 3 sample may be different, but greater line widths and comparable abundances of multiple structures prevent a definitive determination.

For the majority structure in brain-seeded samples, secondary chemical shifts. i.e., differences between observed $^{13}$C chemical shifts and reported shifts for random-coil polypeptides (19), are negative for carbonyl and $\alpha$-carbon sites and positive for $\beta$-carbon sites of all $^{13}$C-labeled residues except V24 and G25, indicating the presence of $\beta$-strand segments that contain F19, A30, I31, L34, and M35. These secondary shifts are qualitatively consistent with the strand-bend-strand conformational motif for A$\beta_{1-40}$ that has been observed in purely synthetic A$\beta_{1-40}$ fibrils (4, 5). However, the precise values of chemical shifts for brain-seeded samples are significantly different from reported shifts in purely synthetic A$\beta_{1-40}$ fibrils (Table S1 and Fig. 4*D*). The root-mean-squared deviation values between the majority signals of brain 1/generation 3 fibrils and reported chemical shifts of synthetic striated ribbon and twisted fibrils (1, 4) are 1.05 and 1.00 ppm, respectively. Thus, although the A$\beta_{1-40}$ peptide in brain-seeded fibrils apparently has the same conformational motif as in previously characterized synthetic fibrils, the details of the full molecular structure are not the same.

Inter-residue sidechain–sidechain contacts within the brain-seeded A$\beta_{1-40}$ fibril structures were probed with a different form of 2D $^{13}$C NMR spectroscopy, using radiofrequency-assisted diffusion (RAD) (20, 21) mixing periods as previously described (1, 4). 2D RAD spectra of brain 1/generation 3 and brain 2/generation 3 samples (Figs. 4*A*, 4*B*) show strong inter-residue crosspeaks between F19 aromatic and I31 aliphatic signals, indicating spatial proximity (within ≈0.6 nm) of these sidechains. F19/I31 crosspeaks are observed only for the majority signals in both brain-seeded samples. This result is further evidence that the two brain-seeded samples have the same majority structure, and that this majority structure is different from purely synthetic fibril structures that have been characterized in detail, in which F19/I31 sidechain–sidechain contacts are not observed (4, 5). 2D RAD spectra of purely synthetic fibrils show F19/L34, but not F19/I31, crosspeaks (Fig. S3).

The 2D RAD spectrum of the control/generation 3 sample (Fig. 4*C*) shows weaker crosspeaks between F19 aromatic signals and I31 aliphatic signals. Volumes for F19-C$_\varepsilon$/I31-C$_\delta$ crosspeaks, normalized to the volumes of F19-C$_\varepsilon$/F19-C$_\alpha$ crosspeaks, are 0.20 ± 0.05, 0.19 ± 0.06, and 0.12 ± 0.02, for 2D RAD spectra of brain 1/generation 3, brain 2/generation 3, and control/generation 3 samples, respectively. In addition, weak F19/V24 crosspeaks are observed in the 2D RAD spectrum of the controls sample but not in spectra of brain-seeded samples.

Additional 2D fpRFDR spectra were obtained from brain 1/generation 3 and brain 2/generation 3 samples with uniform $^{15}$N,$^{13}$C-labeling of D23, K28, G29, I32, and V36 (Fig. S4). Again, spectra of these two samples are nearly identical, with $^{13}$C chemical shifts that differ significantly from those in synthetic striated ribbon and twisted fibrils (Table S1 and Fig. 3*D*). Chemical shifts for D23 indicate a non–$\beta$-strand conformation. Measurements of $^{15}$N-$^{13}$C

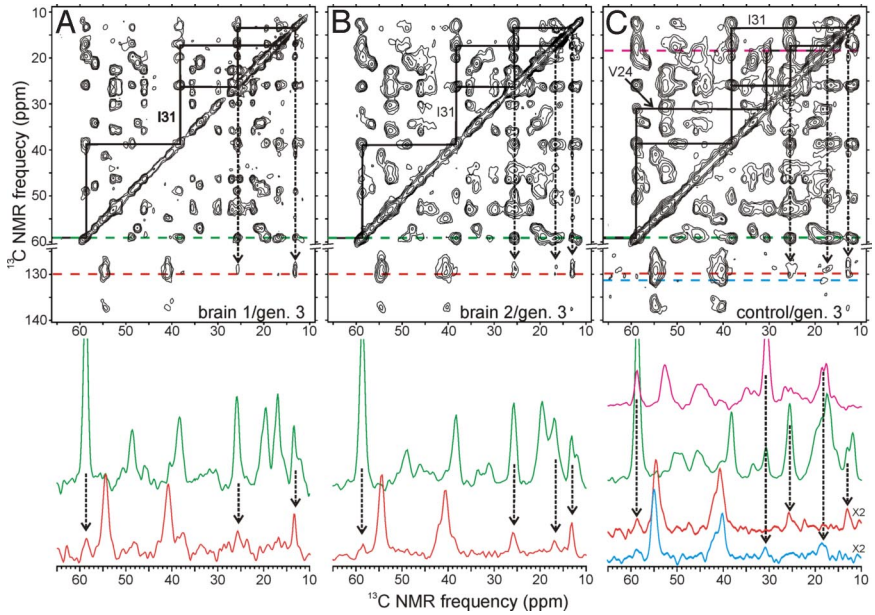


**Fig. 4.** Aromatic and aliphatic regions of 2D solid-state $^{13}$C NMR spectra with 500-millisecond RAD mixing periods. (*A-C*) brain 1/generation 3, brain 2/generation 3, and control/generation 3 fibrils, respectively. Relevant chemical shift assignment paths are shown. Vertical dashed lines with arrowheads indicate spin polarization transfers from aliphatic carbons of I31 (*A-C*) and V24 (*C* only) to F19 aromatic carbons that produce inter-residue crosspeaks and reflect sidechain-sidechain contacts. One-dimensional slices below each two-dimensional spectrum are taken at positions indicated by the color-coded horizontal dashed lines. Green slice, I31 $C_\alpha$; red and blue slices, F19 aromatic; magenta, V24 $C_\gamma$.

dipole–dipole couplings between the K28 sidechain amino group and the D23 sidechain carboxylate group in these samples, using the frequency-selective rotational echo double resonance technique (22), indicate 3.4 ± 0.2 Å $^{15}$N-$^{13}$C distances (Fig. 5*A*), consistent with D23-K28 salt bridge interactions as observed previously in synthetic striated ribbon fibrils (1, 5). Additional measurements of intermolecular $^{13}$C-$^{13}$C dipole–dipole couplings in a brain 1/generation 3 sample with selective $^{13}$C labeling of the V12 carbonyl and the A21 methyl carbon sites, using the PITHIRDS-CT technique (23), indicate 4.8 ± 0.2 Å intermolecular distances for both sites (Fig. 5*B*), establishing an in-register, parallel β-sheet structure as in purely synthetic A$\beta_{1-40}$ fibrils (1, 4, 24).

In existing structural models for purely synthetic A$\beta_{1-40}$ fibrils (4, 5), β-strands formed by residues 10–22 and 30–40 form separate in-register parallel β-sheets, with inter-sheet contacts between odd-numbered sidechains in the N-terminal β-strand and even-numbered sidechains in the C-terminal β-strand. The F19/I31 contacts in Fig. 5 indicate that the C-terminal β-sheet is flipped in the majority brain-seeded structure, placing odd-number sidechains in the N-terminal and C-terminal β-strands in contact with one another. Such a model was suggested in earlier work (see Fig. 4 in Ref. 25), but was not confirmed in more extensive studies of purely synthetic A$\beta_{1-40}$ fibrils (4, 5, 26). Cysteine mutants of A$\beta_{1-40}$ have been found to be capable of such contacts (3), and F19/I31 contacts have been detected by solid-state NMR in fibrils formed by residues 10–40 of β-amyloid (2).

## Discussion

Data presented above show that fibrillar material extracted from AD brain tissue accelerates fibril formation in synthetic A$\beta_{1-40}$ solutions, in the same way that synthetic A$\beta_{1-40}$ fibrils act as seeds for fibril growth (1, 4). These data are consistent with earlier work of Maggio et al., who showed that synthetic β-amyloid peptides bind to AD (but not normal) brain tissue, presumably by adding to fibrils in the tissue (27). Because molecular structures and morphologies of A$\beta_{1-40}$ fibrils have been shown to propagate themselves through multiple generations in seeded growth (1, 4), the molecular structures of brain-seeded A$\beta_{1-40}$ fibrils are likely to correspond to structures in the brains themselves. The similarity of solid-state NMR spectra of brain 1/generation 3 and brain 2/generation 3 samples, together with the observation of greater structural heterogeneity in the control/generation 3 sample, suggests that specific structures are present in AD brains. NMR data for the two AD brain–seeded samples indicate that the same two molecular structures are present in both samples, and that both brain-seeded structures differ from structures that we have characterized in previous studies of purely synthetic A$\beta_{1-40}$ fibrils with striated ribbon and twisted morphologies (4, 5). The predominant structure in brain-seeded samples has the morphology indicated by red arrows in Figs. 1*G* and 1*H*. $^{13}$C NMR chemical shifts indicate a strand-bend-strand conformational motif in the predominant structure. 2D RAD spectra indicate F19/I31 sidechain–sidechain contacts between β-sheets formed by the N-terminal and C-terminal β-strands. MPL data suggest the presence of three molecular layers in the predominant structure.

Our previous work has shown that A$\beta_{1-40}$ fibrils with distinct structures exhibit different levels of toxicity in neuronal cell cultures, raising the possibility that certain fibril structures may be more neurotoxic than others in the brain (1, 4). Results described above indicate the feasibility of testing this proposal by directly comparing molecular structures of brain-seeded fibrils prepared with extracts from different sources of brain tissue, using physical measurements such as solid-state NMR and electron microscopy. For example, fibrils in β-amyloid plaques in AD patients may differ structurally from those in asymptomatic elderly persons, or fibril structure may correlate with the degree of cognitive impairment and neurodegeneration in AD patients.

The precise nature of aggregated β-amyloid that is the primary neurotoxic species in AD is a subject of current debate, with much recent work focusing on nonfibrillar aggregates (11, 17, 28–30). The modest correlation in AD between plaque burden at autopsy and severity of dementia before death (31) is one important motivation for this debate. In addition, although plaques are present throughout the brain at autopsy, AD symptoms (i.e., memory loss and cognitive dysfunction) are associated mainly with the frontal cortex

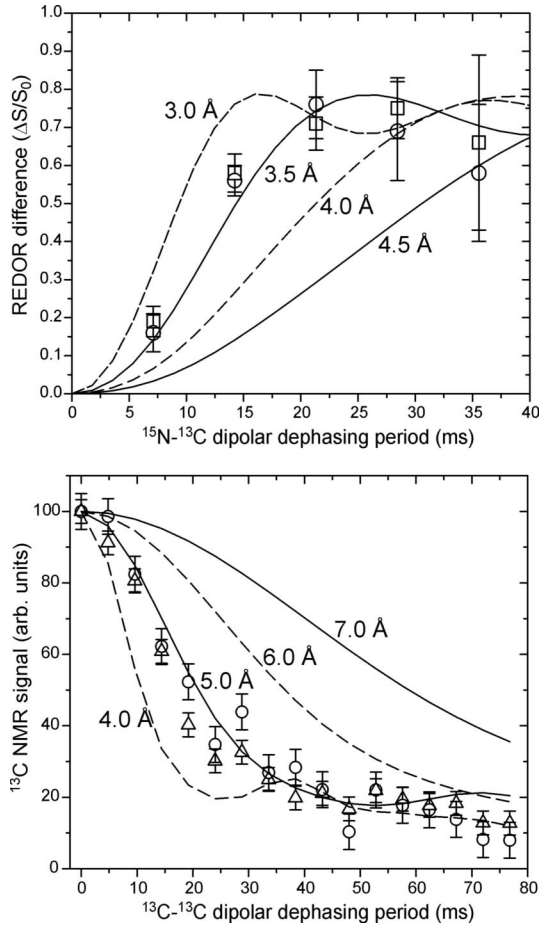


**Fig. 5.** Internuclear distances in brain-seeded A$\beta_{1-40}$ fibrils. (*Upper*) Measurements of $^{15}$N-$^{13}$C dipole-dipole couplings between sidechains of K28 and D23 in brain 1/generation 3 (open squares) and brain 2/generation 3 (open circles) fibrils, using the frequency-selective rotational echo double resonance technique with detection of D23 carboxylate $^{13}$C NMR signals and dephasing by K28 sidechain $^{15}$N nuclei. Comparison with simulated curves for $^{15}$N-$^{13}$C pairs indicates a distance of 3.4 ± 0.2 Å. (*Lower*) Measurements of intermolecular $^{13}$C-$^{13}$C couplings for $^{13}$C labels at the V12 carbonyl (open circles) and A21 methyl (open triangles) sites in brain 1/generation 3 fibrils, using the PITHIRDS-CT technique. Comparison with simulated curves indicates 4.8 ± 0.2 Å intermolecular distances for both sites. Simulations are for linear chains of three $^{13}$C nuclei with initial spin polarization on the central nucleus, and include a 75-millisecond transverse spin relaxation time. Experimental signals are corrected for natural-abundance contributions by subtraction of a 20% (open circles) or 10% (open triangles) constant baseline.

and hippocampus. AD patients do not have clinical signs relating to the occipital lobe, for example, despite that fact that neuritic plaques can be abundant in this region (32, 33). Although these observations may indicate a non-essential role for β-amyloid fibrils, they may also be a consequence of variations in the molecular structure of fibrils among patients and among brain regions (if, in fact, fibrils with different structures have significantly different neurotoxic effects in the brain). Future experiments will address these possibilities. In addition, even if the primary neurotoxic species are nonfibrillar aggregates that are precursors to fibrils, fibril structure may report on precursor structure, given that molecular structural variations in amyloid fibrils arise from structural variations at the nucleation stage (1–3), which precedes the appearance of the fibrils themselves.

Meyer-Luehmann et al. (9) have shown that intracerebral injection of brain extracts from AD patients or aged transgenic mice (APP23 and APPPS1) into young APP23 and APPPS1 mice induces amyloid plaque formation, with histopathological details that depend on both the source and the host. Their observations suggest the presence of structural variations among β-amyloid aggregates in the human and transgenic mouse brains, as well as environmental effects on the propagation of specific structures. Attempts to induce plaque formation in the same mice by intracerebral injection of purely synthetic β-amyloid fibrils were unsuccessful (9), suggesting that their synthetic fibrils were structurally distinct from fibrils in their brain extracts. Overall, these results are consistent with our experiments and with the hypotheses outlined above.

Nilsson et al. have described the use of luminescent conjugated polymers as fluorescent dyes that can differentiate among β-amyloid fibril structures (34). Their experiments on brain tissue from $APP_{Swe}$ transgenic mice show the presence of different fibril structures in different plaque types and in different regions of plaques (core vs. periphery), although the nature of these structural differences is not known. In related work, Sigurdson et al. have shown that binding to different mammalian prion strains induces variations in the fluorescence spectra of luminescent conjugated polymers (35), suggesting a similarity between structural differences that underlie prion strains and structural differences among β-amyloid fibrils in brain tissue.

Finally, our approach to amplification of A$\beta_{1-40}$ fibril quantities by repeated rounds of seeding is similar to the work of Soto et al. and Caughey et al., who have demonstrated the amplification of mammalian prion proteins in protease-resistant form by seeded growth (36, 37), and to that of Colby et al., who have demonstrated seeded growth of recombinant prion protein fibrils by partially purified prions derived from brain tissue (38). The same approach may also be used to identify the molecular structures of polymorphic fibrils associated with other amyloid diseases, such as amylin fibrils in type 2 diabetes (39), by seeding synthetic peptides or recombinant proteins with fibrils extracted from the affected tissue.

## Materials and Methods

**Amyloid Extraction.** Frontal lobe brain tissue was obtained at autopsy from two patients who had been diagnosed with advanced AD. Frontal lobe tissue was chosen because it is abundant and is known to contain a high density of neuritic plaques. Diagnosis was confirmed by histopathological examination of this tissue and other brain tissue. Brains 1 and 2 refer to those of a 90-year-old woman and a 76-year-old man, respectively. No personal descriptors were available to us. Amyloid was extracted essentially as described by Roher et al. (12), except that filtration using steel meshes and final dissolution of the material in formic acid were not performed. Details are given in SI Text. Typically, 80 μg of protein (BCA and Bradford assays) was obtained from 30 g of brain tissue. Extracted material was divided into aliquots containing 8–10 μg of protein and stored at −80 °C until needed.

Frontal lobe brain tissue was also obtained from autopsies of two nondemented patients who died of conditions unrelated to AD, a 56-year-old woman and a 25-year-old man. In both of these cases, application of the same extraction procedure yielded roughly 22 μg of protein from 20 g of tissue. TEM of this material showed only nonfibrillar particles. AD Brain 2 was from National Development and Research Institutes, Inc. All other brain tissue was from The University of Chicago Hospitals.

**ThT Fluorescence.** Fibrillogenesis kinetics experiments used 100 μM of monomeric synthetic A$\beta_{1-40}$ in 10 mM sodium phosphate, pH 7.40 (14). Seeds were either aliquots from brain tissue or synthetic A$\beta_{1-40}$ fibrils, produced as described elsewhere (14). Seeds were suspended in 25 μl of 10 mM sodium phosphate, pH 7.40, and probe sonicated for 60 seconds at 20 °C before addition to a fresh A$\beta_{1-40}$ solution. Seeds represented ≈5% of the total peptide mass. Relative fibril quantities at each time point were measured by adding 10 μl aliquots of peptide solutions to 1 ml of 10 μM ThT solution and recording fluorescence at 490 nm with excitation at 446 nm (Hitachi F2000 fluorimeter).

**Preparation of Solid-State NMR Samples.** A$\beta_{1-40}$ (sequence DAEFRHDSGY EVHHQKLVFF AEDVGSNKGA IIGLMVGGVV) was synthesized and purified as previously described (1). Monomeric A$\beta_{1-40}$ solutions were prepared immediately before seeding by dissolving synthetic peptide at 5.8 mM in dimethyl sulfoxide (DMSO), diluting to 210 μM in pH 7.40 buffer solution (10 mM phosphate, 0.01% $NaN_3$), dialyzing for 1 hour against pH 7.40 buffer, and filtering with 0.22 μm

filters (Millipore Millex). Seeds (≈5% by $A\beta_{1-40}$ molecules) were prepared by probe sonication of the previous fibril generation (Branson model 250 sonifier, lowest power, 10% duty factor, 30 seconds). For seeding of generation 1, brain material containing ≈9 $\mu$g of fibrils was dispersed in 100 $\mu$l of pH 7.40 buffer by probe sonication for 60 seconds immediately before addition to 198 $\mu$l of 210 $\mu$M monomeric $A\beta_{1-40}$ solution. For control/generation 1, a blank 100-$\mu$l buffer aliquot was treated identically before addition to a monomeric $A\beta_{1-40}$ solution.

Generation 1 solutions were incubated quiescently at room temperature for 1 month before sonication to generate seeds for generation 2. This extended incubation period and quiescent conditions were chosen to permit all structures in the brain extract to act as seeds and to ensure full conversion of synthetic $A\beta_{1-40}$ to fibrillar form. To accelerate fibril formation, minimize possible contributions from unseeded fibril growth, and reduce preferential propagation of specific amyloid structures, generations 2 and 3 were ''self-seeded'' 4 hours after initial seeding, i.e., aliquots (5% by volume) were taken from the incubating solutions, bath sonicated (Cole-Parmer ultrasonic cleaner) in 1-ml tubes for 3 minutes, and then returned to the incubating solutions. Self-seeded solutions were then incubated for 24 hours before electron microscopy, solid-state NMR, or sonication for the next generation. For solid-state NMR, generation 3 fibrils were pelleted by ultracentrifugation for 20 minutes at 175,000 *g*, resuspended in deionized water, frozen in liquid nitrogen, and lyophilized. Lyophilized fibril samples (≈4 mg each) were packed in 3.2 mm MAS NMR rotors and rehydrated with 0.5–1.0 $\mu$l of deionized water per milligram of $A\beta_{1-40}$.

**Electron Microscopy.** TEM images were recorded with an FEI Morgani microscope operating at 80 kV. Fibril solutions were diluted in deionized water to ≈20 $\mu$M $A\beta_{1-40}$ concentration. Aliquots (5 $\mu$l) were adsorbed for 2 minutes to freshly glow-discharged carbon films (≈5 nm thickness, supported by lacey carbon on a 300-mesh copper grid) and blotted with filter paper. After rinsing with deionized water (5 $\mu$l for 1 minute) and blotting, samples were stained with 3% uranyl acetate (5 $\mu$l for 1 minute), blotted, and air-dried.

Brain extract was probe sonicated briefly (10 seconds, lowest power, 10% duty factor) before adsorption to carbon films. Without probe sonication, amyloid fibrils in brain extract were masked by nonfibrillar material and could not be observed clearly by TEM.

The brain-seeded sample for EFTEM measurements was prepared in a similar manner to the TEM samples, but with thinner carbon films (3 nm), co-adsorption of tobacco mosaic virus (TMV) as a mass standard (131 kDa/nm), no stain, and extra rinsing steps to remove nonfibrillar material. EFTEM images were recorded as described by Feja et al. (16), using an FEI Tecnai TF30 microscope at 300 kV, with an incident dose of ≈2000 electrons/nm$^2$ and a 15–35 eV energy loss range, which includes the plasmon maximum at 25 eV.

**Solid-State NMR.** Measurements were performed in a 14.1-T field (150.7-MHz $^{13}$C NMR frequency) with a Varian InfinityPlus spectrometer and Varian 3.2 mm MAS NMR probes. 2D $^{13}$C NMR spectra were recorded with fpRFDR mixing (18) (23.00 kHz MAS, 13.0-microsecond $^{13}$C $\pi$ pulses, 1.39-millisecond mixing period or 14.00 kHz MAS, 20.0-microsecond $^{13}$C $\pi$ pulses, 2.29-millisecond mixing period) or at 20.00 kHz MAS frequency with RAD mixing (20, 21) (500-millisecond mixing period), with other conditions as described elsewhere (1, 2, 4, 5). Frequency-selective rotational echo double resonance and PITHIRDS-CT data were obtained as previously described (4, 5, 23).

**ACKNOWLEDGMENTS.** This work was supported by the Intramural Research Programs of the National Institute of Diabetes and Digestive and Kidney Diseases (to A.K.P. and R.T.); by the National Institute of Biomedical Imaging and Bioengineering of the National Institutes of Health (to R.D.L.); and by the National Institutes of Health (grant NS042852, to S.C.M.); and by the Alzheimer's Association (grant IIRG-06–27794, to S.C.M.).

1. Petkova AT, et al. (2005) Self-propagating, molecular-level polymorphism in Alzheimer's $\beta$-amyloid fibrils. *Science* 307:262–265.
2. Paravastu AK, Petkova AT, Tycko R (2006) Polymorphic fibril formation by residues 10–40 of the Alzheimer's $\beta$-amyloid peptide. *Biophys J* 90:4618–4629.
3. Wetzel R, Shivaprasad S, Williams AD (2007) Plasticity of amyloid fibrils. *Biochemistry* 46:1–10.
4. Paravastu AK, Leapman RD, Yau W-M, Tycko R (2008) Molecular structural basis for polymorphism in Alzheimer's $\beta$-amyloid fibrils. *Proc Natl Acad Sci USA* 105:18349–18354.
5. Petkova AT, Yau WM, Tycko R (2006) Experimental constraints on quaternary structure in Alzheimer's $\beta$-amyloid fibrils. *Biochemistry* 45:498–512.
6. Wickner R, et al. (2004) Prions: Proteins as genes and infectious entities. *Genes Dev* 18:470–485.
7. Caughey B, Raymond GJ, Bessen RA (1998) Strain-dependent differences in $\beta$-sheet conformations of abnormal prion protein. *J Biol Chem* 273:32230–32235.
8. Chien P, Weissman JS, De Pace AH (2004) Emerging principles of conformation-based prion inheritance. *Annu Rev Biochem* 73:617–656.
9. Meyer-Luehmann M, et al. (2006) Exogenous induction of cerebral $\beta$-amyloidogenesis is governed by agent and host. *Science* 313:1781–1784.
10. Hardy J, Selkoe DJ (2002) The amyloid hypothesis of Alzheimer's disease: Progress and problems on the road to therapeutics. *Science* 297:353–356.
11. Lesne S, et al. (2006) A specific amyloid-$\beta$ protein assembly in the brain impairs memory. *Nature* 440:352–357.
12. Roher AE, Kuo YM (1999) in *Methods in Enzymology*, ed. Wetzel, R. (Academic, San Diego), Vol. 309, pp. 58–67.
13. Roher AE, et al. (1993) Structural alterations in the peptide backbone of $\beta$-amyloid core protein may account for its deposition and stability in Alzheimer's disease. *J Biol Chem* 268:3072–3083.
14. Sciarretta KL, Gordon DJ, Petkova AT, Tycko R, Meredith SC (2005) A$\beta$40-lactam(D23/K28) models a conformation highly favorable for nucleation of amyloid. *Biochemistry* 44:6003–6014.
15. Qahwash I, et al. (2007) Site-specific effects of peptide lipidation on $\beta$-amyloid aggregation and cytotoxicity. *J Biol Chem* 282:36987–36997.
16. Feja B, Durrenberger M, Muller S, Reichelt R, Aebi U (1997) Mass determination by inelastic electron scattering in an energy-filtering transmission electron microscope with slow-scan CCD camera. *J Struct Biol* 119:72–82.
17. Goldsbury C, Frey P, Olivieri V, Aebi U, Muller SA (2005) Multiple assembly pathways underlie amyloid-$\beta$ fibril polymorphisms. *J Mol Biol* 352:282–298.
18. Ishii Y (2001) $^{13}$C-$^{13}$C dipolar recoupling under very fast magic angle spinning in solid state nuclear magnetic resonance: Applications to distance measurements, spectral assignments, and high-throughput secondary-structure determination. *J Chem Phys* 114:8473–8483.
19. Wishart DS, Bigam CG, Holm A, Hodges RS, Sykes BD (1995) $^{1}$H, $^{13}$C and $^{15}$N random coil NMR chemical shifts of the common amino acids. 1. Investigations of nearest-neighbor effects. *J Biomol Nucl Magnet Reson* 5:67–81.
20. Morcombe CR, Gaponenko V, Byrd RA, Zilm KW (2004) Diluting abundant spins by isotope edited radio frequency field assisted diffusion. *J Am Chem Soc* 126:7196–7197.
21. Takegoshi K, Nakamura S, Terao T (2001) $^{13}$C-$^{1}$H dipolar-assisted rotational resonance in magic angle spinning NMR. *Chem Phys Lett* 344:631–637.
22. Jaroniec CP, Tounge BA, Herzfeld J, Griffin RG (2001) Frequency selective heteronuclear dipolar recoupling in rotating solids: Accurate $^{13}$C-$^{15}$N distance measurements in uniformly $^{13}$C,$^{15}$N-labeled peptides. *J Am Chem Soc* 123:3507–3519.
23. Tycko R (2007) Symmetry-based constant-time homonuclear dipolar recoupling in solid state NMR. *J Chem Phys* 126:064506.
24. Balbach JJ, et al. (2002) Supramolecular structure in full-length Alzheimer's $\beta$-amyloid fibrils: Evidence for a parallel $\beta$-sheet organization from solid state nuclear magnetic resonance. *Biophys J* 83:1205–1216.
25. Petkova AT, et al. (2002) A structural model for Alzheimer's $\beta$-amyloid fibrils based on experimental constraints from solid state NMR. *Proc Natl Acad Sci USA* 99:16742–16747.
26. Luhrs T, et al. (2005) 3D structure of Alzheimer's amyloid-$\beta$(1–42) fibrils. *Proc Natl Acad Sci USA* 102:17342–17347.
27. Esler WP, et al. (1996) *In vitro* growth of Alzheimer's disease $\beta$-amyloid plaques displays first-order kinetics. *Biochemistry* 35:749–757.
28. Chen YR, Glabe CG (2006) Distinct early folding and aggregation properties of Alzheimer amyloid-$\beta$ peptides A$\beta$40 and A$\beta$42: Stable trimer or tetramer formation by A$\beta$42. *J Biol Chem* 281:24414–24422.
29. Bitan G, et al. (2003) Amyloid $\beta$-protein (A$\beta$) assembly: A$\beta$40 and A$\beta$42 oligomerize through distinct pathways. *Proc Natl Acad Sci USA* 100:330–335.
30. Selkoe DJ (2008) Soluble oligomers of the amyloid $\beta$-protein impair synaptic plasticity and behavior. *Behav Brain Res* 192:106–113.
31. Berg L, et al. (1998) Clinicopathologic studies in cognitively healthy aging and Alzheimer disease: Relation of histologic markers to dementia severity, age, sex, and apolipoprotein E genotype. *Arch Neurol* 55:326–335.
32. McKee AC, et al. (2006) Visual association pathology in preclinical Alzheimer disease. *J Neuropath Exp Neurol* 65:621–630.
33. Thal DR, Rub U, Orantes M, Braak H (2002) Phases of a $\beta$-deposition in the human brain and its relevance for the development of ad. *Neurology* 58:1791–1800.
34. Nilsson KPR, et al. (2007) Imaging distinct conformational states of amyloid-$\beta$ fibrils in Alzheimer's disease using novel luminescent probes. *ACS Chem Biol* 2:553–560.
35. Sigurdson CJ, et al. (2007) Prion strain discrimination using luminescent conjugated polymers. *Nat Methods* 4:1023–1030.
36. Atarashi R, et al. (2008) Simplified ultrasensitive prion detection by recombinant PrP conversion with shaking. *Nat Methods* 5:211–212.
37. Saa P, Castilla J, Soto C (2006) Ultra-efficient replication of infectious prions by automated protein misfolding cyclic amplification. *J Biol Chem* 281:35245–35252.
38. Colby DW, et al. (2007) Prion detection by an amyloid seeding assay. *Proc Natl Acad Sci USA* 104:20915–20919.
39. Luca S, Yau WM, Leapman R, Tycko R (2007) Peptide conformation and supramolecular organization in amylin fibrils: Constraints from solid state NMR. *Biochemistry* 46:13505–13522.